Improving mechanical properties of friction-stir-spot-welded advanced ultra-high-strength steel with additional water cooling

Z. W. Wang, G. N. Ma, B. H. Yu, P. Xue, G. M. Xie, H. Zhang, D. R. Ni, B. L. Xiao & Z. Y. Ma

Published online: 25 Dec 2019.

Submit your article to this journal

Article views: 176

View related articles

View Crossmark data

Citing articles: 4 View citing articles

The Institute of Materials,
Minerals and Mining

Taylor & Francis
Taylor & Francis Group

Check for updates

Improving mechanical properties of friction-stir-spot-welded advanced ultra-high-strength steel with additional water cooling

Z. W. Wang[a,b], G. N. Ma[a,b], B. H. Yu[a], P. Xue[a], G. M. Xie[c], H. Zhang[a], D. R. Ni[a], B. L. Xiao[a] and Z. Y. Ma[a]

[a]Shenyang National Laboratory for Materials Science, Institute of Metal Research, Chinese Academy of Sciences, Shenyang, People's Republic of China; [b]School of Materials Science and Engineering, University of Science and Technology of China, Shenyang, People's Republic of China; [c]State Key Laboratory of Rolling and Automation, Northeastern University, Shenyang, People's Republic of China

ABSTRACT
1.2 mm thick DP1180 advanced ultra-high-strength steel were successfully friction stir spot welded (FSSWed) with additional water cooling. No hook defect and obvious keyhole were observed in the spot joints when using a specially designed WC-Co tool. Softening of the heat-affected zone was substantially suppressed and the lap shear strength of the joints was obviously enhanced via water cooling. The enhanced strength of water-cooled joints was attributed to the grain refinement, the formation of the untempered martensite and the effective restraint of tool softening underwater. Accordingly, the maximum lap shear strength of 17.9 kN was obtained for the water-cooled joint. This study provides a novel strategy to enhance the strength of the FSSW joints for high-strength steels.

Introduction

Advanced high-strength steels (AHSSs) are developed for the automotive industry to achieve lighter auto-body with higher strength. In recent years, several advanced ultra-high-strength steels with tensile strength over 1 GPa have been produced to further reduce the weight of vehicle structures [1]. As a typical AHSS, martensite-ferrite dual-phase (DP) steels have been widely used in the automotive industry for its outstanding comprehensive properties. For the joining of DP steels, coarse and hard martensite phase could be easily formed in the fusion zone when fusion welding techniques were adopted [2–6]. Meanwhile, severe softening usually occurred in the heat-affected zone (HAZ), especially for the ultra-high-strength DP steel [3,7].

Friction stir spot welding (FSSW), a variant of friction stir welding (FSW), is a solid-state welding technique with low heat input, where severe plastic deformation is involved simultaneously to produce significant grain refinement. Therefore, FSSW is expected to be able to achieve optimised DP steels joints by controlling the deformation, temperature and cooling rate [8,9]. So far, many researchers have attempted to perform FSSW on DP steels and obtained acceptable lap shear strengths. However, some problems such as severe HAZ softening and poor bonding property also existed, which cannot be ignored for practical application. In the study on FSSW of DP980 steel by Saunders et al. [10], high heat input parameters with high rotation rates of 2500–6000 rev min^{-1} were used and the joint showed a poor lap shear strength, which was due to the broad softened HAZ as well as the narrow bonding area.

It is well known that reducing the heat input can restrain the softening of the HAZ. As for FSW, reducing the rotation rate, increasing the welding speed and applying additional cooling have been proven to be useful methods to reduce the heat input. Some recent reports showed that the mechanical properties of FSW joints could be considerably enhanced via additional water cooling, which was related to the amelioration of heat-induced softening. Up to now, FSW with water cooling has been successfully implemented to join various materials such as pure copper [11], aluminium alloys [12–14], titanium alloy [15] and stainless steel [16]. However, there are no reports on the FSW of AHSS by adopting additional cooling, and the mechanisms of strength improvement and the microstructural evolution during welding have not yet been clarified.

During traditional FSSW, one problem is that the hook defect and keyhole were usually formed due to the existence of stir pin, which resulted in seriously decreased mechanical properties [10,17–20]. Some researchers have attempted to use a pinless tool or refilling process to eliminate the keyhole [21,22]. However, the hook defect was difficult to eliminate due to the intense material flow along the vertical direction. Another problem is the high tool cost which restricts the wide application for the FSSW of steels.

Table 1. Chemical composition of DP1180 steel, wt-%.

C	Mn	Si	Cr	Mo	Cu	Al	S	P	Fe
0.18	2.4	0.60	0.02	0.01	0.02	0.05	0.005	0.01	Bal.

Table 2. Detailed FSSW parameters used in this study.

Rotation rate (rev min^{-1})	Plunge speed (mm min^{-1})	Plunge depth (mm)	Dwell time (s)	Welding environment	Sample ID
400	5	1	10	Air	400-A
400	5	1	10	Water	400-W
600	5	1	10	Air	600-A
600	5	1	10	Water	600-W

Currently used W-Re and PCBN tools have shown better high-temperature properties such as strength and wear resistance than cemented carbide tools during FSW [10,20,23,24], but their costs are too high for manufacturing. However, if the welding heat input could be effectively reduced, the service property and life of the cemented carbide (like WC-Co) tools are expected to improve.

In the present study, an ultra-high-strength DP steel was subjected to FSSW at a reduced rotation rate and additional cooling to reduce the heat input. A specially designed low-cost WC-Co tool with concave shoulder and zero-length pin was used to verify the feasibility of practical application. The aim of this study is (a) to improve the joint strength by eliminating the spot welding defects such as hook and keyhole and (b) understand the mechanisms of strength improvement and microstructural evolution of FSSW joints.

Experimental procedures

Uncoated cold-rolled DP1180 steel sheets were used with a nominal thickness of 1.2 mm. The chemical composition is shown in Table 1. Spot welding was performed by a displacement-controlled FSW machine and the schematic diagram of the welding process is shown in Figure 1(a). Additional water cooling was used during welding, as sketched in Figure 1(b). Two steel sheets with 110 mm in width and 300 mm in length were first fixed in a water trough and flowing water was used during subsequent welding. For comparison, air cooling FSW was performed as well and the detailed welding parameters are listed in Table 2. The shoulder diameter of the WC-Co tool was 12 mm and the root diameter and length of the tapered pin were 4.5 mm and zero, respectively.

After FSSW, the characterisation and analyses on the cross section of the spot weld were carried out by optical microscopy (OM), scanning electron microscope (SEM) and transmission electron microscopy (TEM). The tensile specimens were cut into 16 mm in width and 110 mm in length with a lap width of 20 mm. A tensile speed of 1 mm min^{-1} was used during the tensile shear test with an Instron 8801 machine. The Vickers microhardness was tested on the OM specimens along the middle line of the upper sheet under 200 g load with a spacing of 0.5 mm between two adjacent points.

Results and discussion

### Formation features of the joints

Typical appearances of the FSSW joints under two different welding environments are shown in Figure 2. Mussy flash and malformed burr around the outer edge of the shoulder were obvious in the air-cooled joint (Figure 2(a)). The flash was formed from the extruded material by the plunging action of the rotating shoulder. Compared with the air-cooled joint, the flash appearance was improved and the burr was eliminated for the water-cooled joint (Figure 2(b)). In addition, the spot surface with bluish and orange colour of 600-A sample indicates that serious oxidation occurred during welding. However, no obvious oxidation feature was observed in the 600-W sample on account of the efficient isolation of the atmosphere and the reduction of welding temperature under the water.

Figure 3 shows the cross-sectional morphologies of the typical FSSW joints. Similar to previous studies of
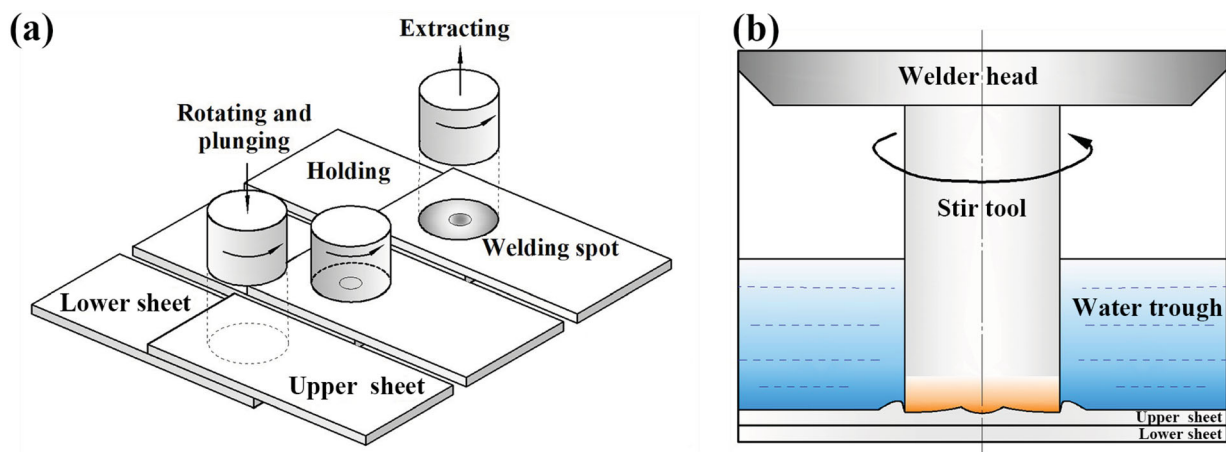
Figure 1. Schematic diagrams of (a) FSSW process, (b) water cooling spot welding with a water trough.
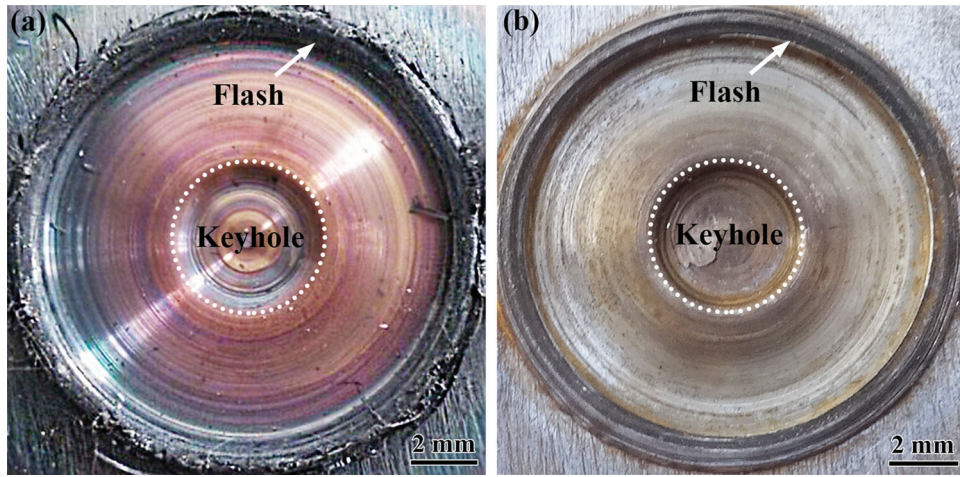
Figure 2. Appearances of the spot joints: (a) 600-A, (b) 600-W.
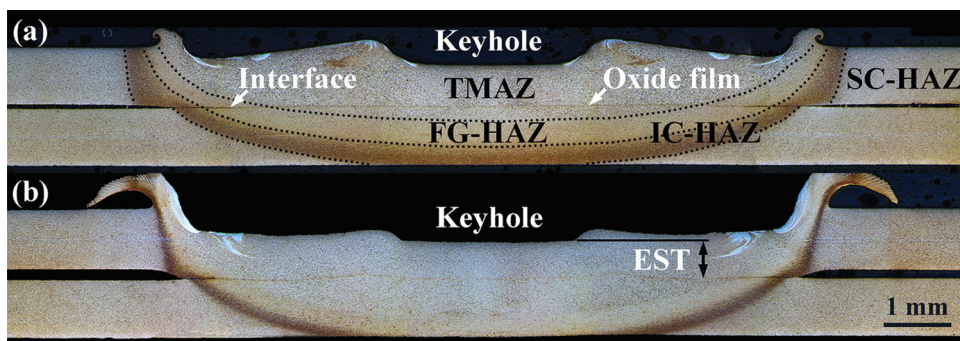
**Figure 3.** Cross-sectional morphologies of the typical joints: (a) 600-A, (b) 600-W.

FSSW, the present spot joints could be divided into three regions by their different structural features, i.e. thermo-mechanical-affected zone (TMAZ), HAZ and parent metal (PM) [20,25,26]. As shown in Figure 3(a), the HAZ could be particularly partitioned into three sub-zones by different suffering temperatures, i.e. fine grain HAZ (FG-HAZ) with the peak temperature over A_{c3} phase transformation point, inter-critical HAZ (IC-HAZ) with the peak temperature between A_{c1} and A_{c3} and sub-critical HAZ (SC-HAZ) with the peak temperature under A_{c1}, respectively. It should be noted that by using forced water cooling, the area proportion of HAZ in the weld zone was distinctly diminished (Figure 3(b)).

Combined with Figures 2 and 3, the zero-length pin used in this study caused only a shallow keyhole on the upper sheet with a similar shape to the stir tool. Obviously, the hook defect was not found in all joints. However, the penetrating oxide films could be detected throughout the TMAZ, which indicated weak bonding of the original sheets interface. In general, the weak bonding could be verified by the discontinuous or line-shape oxide films in the TMAZ, which implied dissatisfactory material flow during welding. Similar phenomena have been observed in the pinless FSSW of aluminium [22]. It should be noted that the oxide films in the water-cooled joints were unapparent.

Outward the TMAZ, the original interface was easily observed in the HAZ without any combination of the two sheets. In addition, if adequate joining of interface in the TMAZ was presupposed, an important variable which was called effective sheet thickness (EST, as shown in Figure 3(b)) could be used to evaluate the lap shear property of FSSW joint because it decides the load-bearing area [27,28]. For instance, the EST for 400-W and 600-W joints in this study was 0.76 and 0.78 mm, respectively.

Microstructural characteristics and evolution

Figure 4 shows the cross-sectional metallographic structures of the FSSW joints under various parameters. It can be seen that the TMAZ (Figure 4(b–e)) exhibited martensite (M) with a larger grain size compared with the fine DP structures in the PM (Figure 4(a)). However, the grain size in the HAZ was similar to the PM (Figure 4(f–h)). The cold-rolled structures of the PM were unstable for containing ultrafine martensite and ferrite (F) phases, subgrains and dislocations. Therefore, it was very sensitive to the thermal-mechanical process. During the FSSW process, the material in the TMAZ was heated to the highest temperature and stayed for over 10 s. The ultrafine grains had enough driving force and time to grow. Though the stir tool
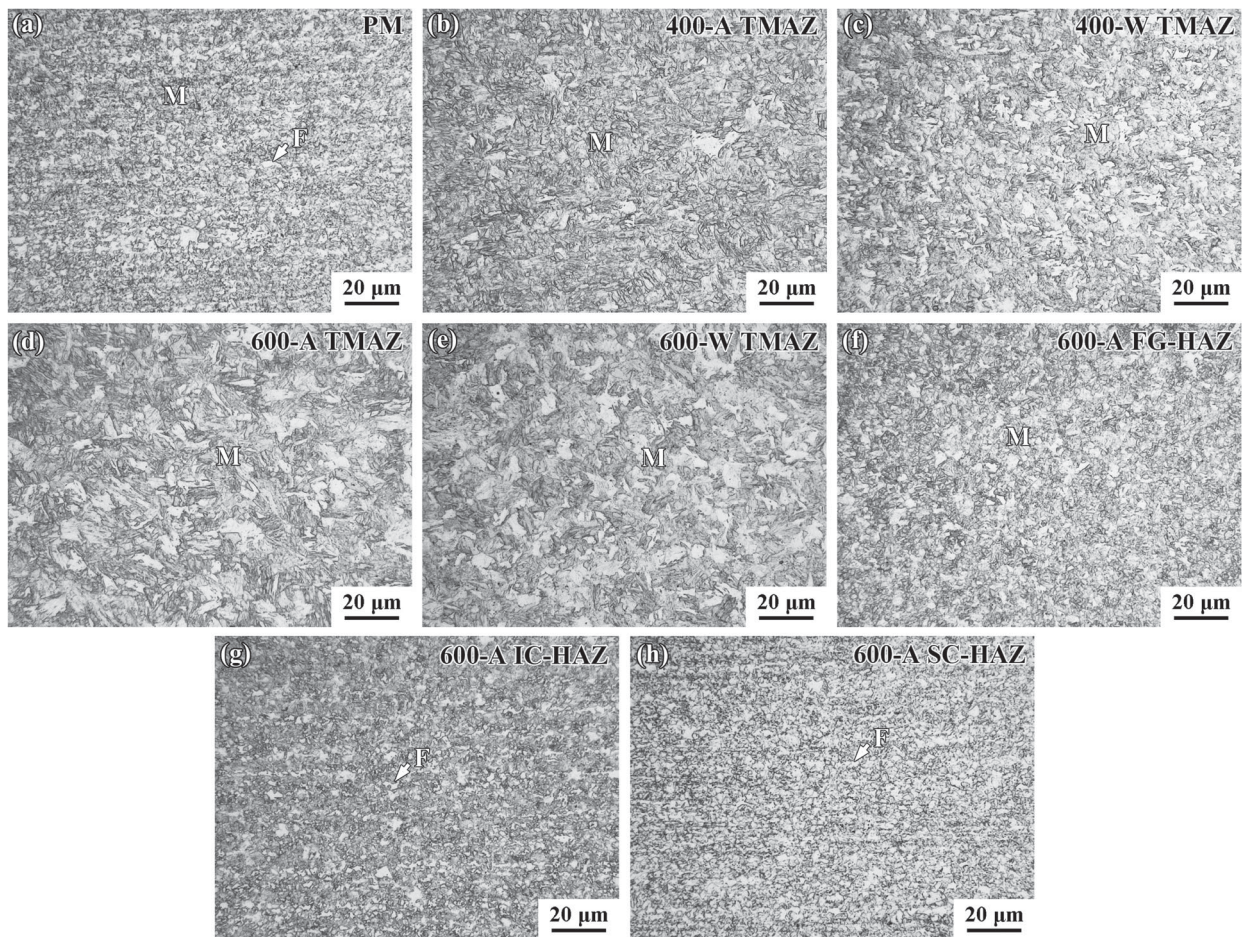
Figure 4. Optical micrographs showing the microstructures of (a) PM, (b)-(e) TMAZ of 400-A, 400-W, 600-A and 600-W joints, (f)-(h) FG-HAZ, IC-HAZ and SC-HAZ of 600-A joint.

could provide plastic deformation and recrystallised grain refining effect, the microstructure of the TMAZ was still coarser than that of the PM.

The FG-HAZ was adjacent to the TMAZ and less affected by heat with the peak temperature lower than that in the TMAZ. Thus, the microstructure showed finer martensite in this region as shown in Figure 4(f). For the IC-HAZ, the original PM was annealed and quenched in the ferrite-austenite 2-phase field. Nemaline ferrite was found in the martensite matrix and its distribution was similar to that of the PM (Figure 4(g)). The SC-HAZ only underwent the tempering process without ferrite-austenite transformation. Owing to the reversion and recrystallisation of deformed grains and tempering of martensite, fine ferrite was generated and carbide particles could be easily precipitated in this region (Figure 4(h)). Specified explanation of the microstructural evolution in the sub-HAZs could be found in our previous work [29].

SEM images of the PM and TMAZs are shown in Figure 5. The TMAZ was composed of full lath martensite and finer structure was obtained under water cooling. This indicated that the peak temperatures in the TMAZs of all joints exceeded A_{c3} and the austenitised structure was transformed into martensite under subsequent cooling. When forced water cooling was applied, the peak temperature and its holding time were reduced significantly. Thus, the austenite grains were prevented from rapid coarsening and resulted in fine martensite in 400-W and 600-W joints (Figure 5(c,e)). In addition, self-tempering is a well-known phenomenon in mild steel and generates tempered martensite (also named lower bainite) proceeding in the quenching process [30]. Thus, the decomposition of martensite occurred ineluctably and a large number of carbide particles could be found in the TMAZs as shown in Figure 5(b,d). However, by greatly increased cooling rate and decreased holding time, the precipitation of carbide was restricted and carbide particles were hard to observe in 400-W and 600-W samples. Meanwhile, the untempered martensite showed smoother appearance in Figure 5(c,e).

Additionally, in order to understand the microstructural features of the joints, TEM images in the TMAZs of 400-A, 600-A and 600-W joints are shown in Figure 6. For the 400-A joint showed in Figure 6(a,b), lath martensite with a lath width below 200 nm was easily observed and obvious distribution of carbide particles could be detected in the matrix of martensite. The bright-field TEM image in Figure 6(b) shows precipitations of acicular and globular carbide particles
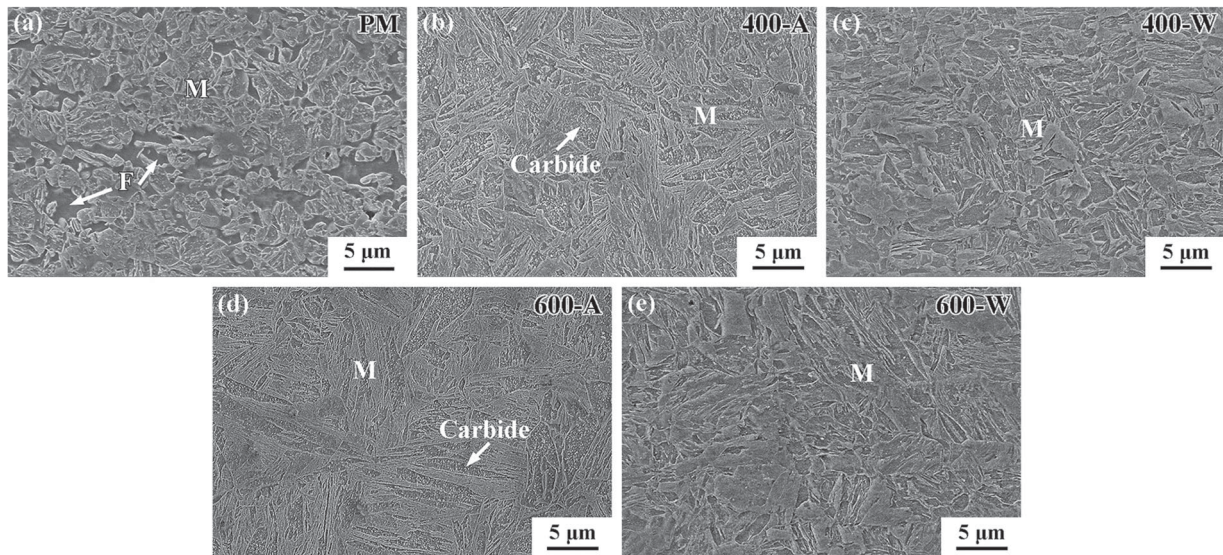
Figure 5. SEM images of (a) PM, (b)-(e) TMAZs of 400-A, 400-W, 600-A and 600-W samples.
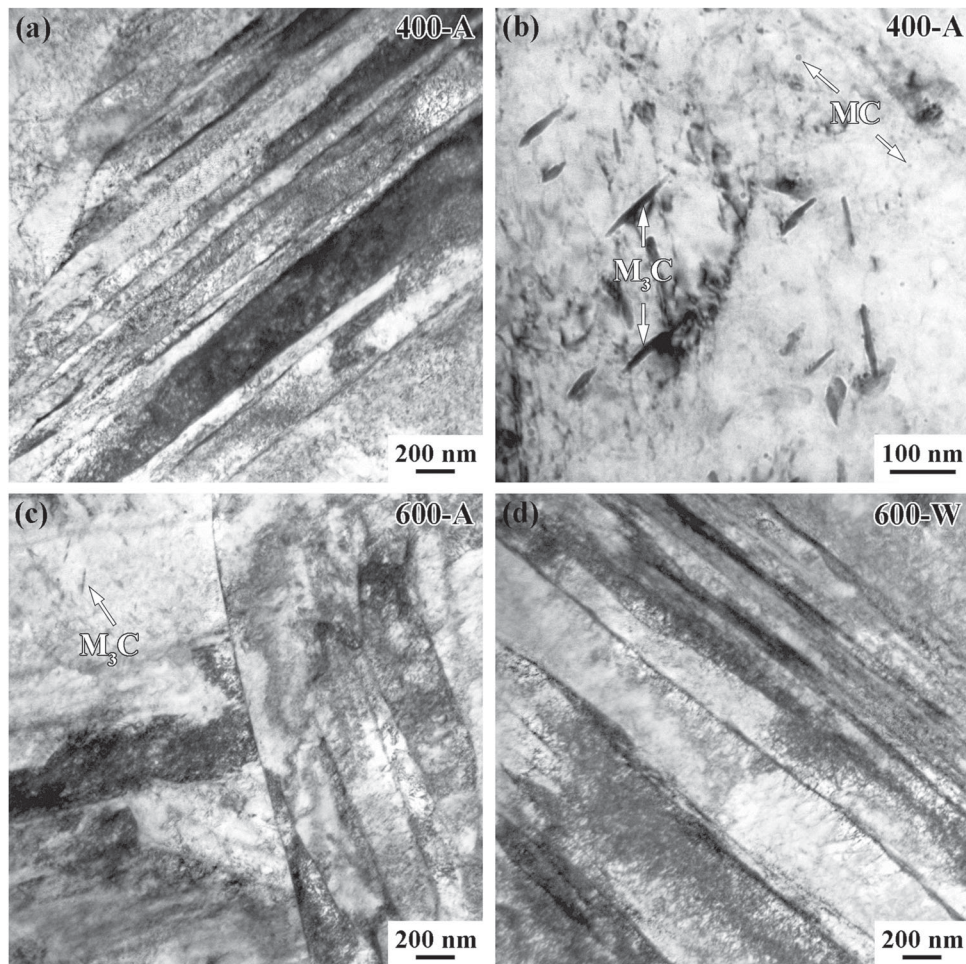
Figure 6. TEM images of TMAZs of (a)-(b) 400-A, (c) 600-A, (d) 600-W samples.

M_3C and MC, as reported in Ref. [31]. For the 600-A joint showed in Figure 6(c), wider martensite laths and more obvious carbide particles could be found due to higher peak temperature in this region than that for 400-A joint. By the means of increasing cooling rate and reducing quenching temperature with water cooling, carbide particle was hard to notice in the 600-W joint, which was consistent with the SEM results showed in Figure 5.

Mechanical properties

Figure 7(a) shows the typical hardness distribution of the FSW joints. Owing to the generation of full
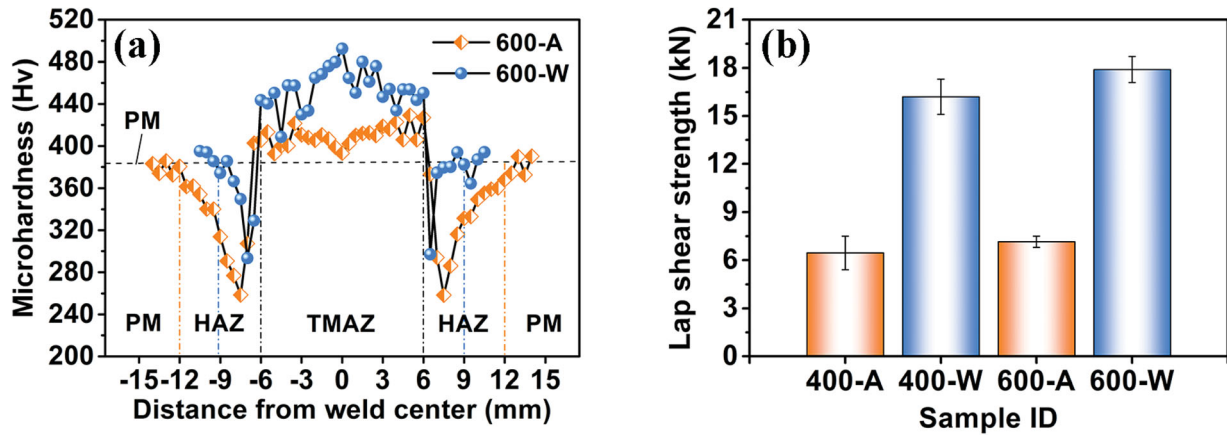
Figure 7. Hardness profiles of typical joints (a) and average lap shear strength of the FSSW joints (b).

Table 3. Lap shear strength and detailed process conditions of the reported FSSW DP steel joints.

| Materials	Sheet thickness (mm)	Tool materials	Rotation rate (rev min^{-1})	Lap shear strength (kN)	References
DP600	1.6	PCBN	1500	10.2	[20]
DP600	1.2	W-25Re	3000	11	[25]
DP780	1.5	PCBN	800	14.7	[32]
DP780	1.5	W-25Re	1000	18.2	[33]
DP980	1.4	PCBN	1500	~14	[23]
DP980	1.2	Si$_3$N$_4$	3000	11.9	[34]
DP980	1.2	PCBN	6000	12.9	[10]
DP1200	2	WC-Co	1000	16.7	[35]
DP1180	1.2	WC-Co	600	17.9	This work

martensite structure, the TMAZ of 600-A joint owned the average hardness of 409 Hv which was slightly higher than that of the PM (383 Hv). The HAZ showed the lowest hardness (258 Hv) of the joint. This is mainly because that soft ferrite increased in the IC-HAZ and the tempering transformation of martensite occurred in the SC-HAZ [29]. For the 600-W joint, the TMAZ showed much higher hardness than that of the 600-A joint with an average hardness value of up to 455 Hv. This should be caused by the decrease of the grain size and the generation of carbon supersaturated martensite. Compared with that of the 600-A joint, the minimum hardness value in the HAZ of 600-W joint increased to 295 Hv with the width being shrunk nearly by half. Thus, the tempering of martensite was availably inhibited and the softening of the HAZ was ameliorated by using forced water cooling.

The lap shear strength of the joints is presented in Figure 7(b). The result shows that the lap shear strength of the 400-A and 600-A joints was 6.5 and 7.2 kN, respectively. By comparison, the lap shear strength significantly increased up to 16.2 and 17.9 kN for the 400-W and 600-W joints, respectively. Table 3 summarises the lap shear strength and detailed process conditions of different FSSW DP steel joints in the published references. Compared to the previously reported FSSW DP steel joints, higher or equivalent lap shear strength was obtained in this study, by applying a low heat input condition and cheap WC-Co tool.

To understand why the joining strength was greatly improved in the present study, the fractured joints were analysed and two typical failed samples are shown in Figure 8. The air-cooled joint was directly peeled off along the original interface (Figure 8(a)) and exhibited low lap shear strength. The water-cooled joint was torn around the internal weld core (Figure 8(b)) with the joint strength being over twice than that for the air-cooled joint. Obviously, the lap interface forming played a significant role in influencing the strength of the joints.

Closely related to the interface forming, material flow determines the evolution of the original interface. The inappropriate flowing patterns could lead to various defects such as hook [27], void and weak bonding [36,37]. For example, the conventional FSSW tool with long stir pin could produce poor joint with narrow effective bonding width (EBW, as shown in Figure 9(a)), which was attributed to the existence of keyhole [20,23,32–34]. In order to eliminate the keyhole and increase the EBW, re-filling FSSW technology was developed. However, it was easy to cause plastic material flow along the vertical direction and to form a large hook defect (Figure 9(b)) [21], which induced premature failure of joint with low strength. From then on, the pinless tool was attempted to reduce the size of the hook defect. However, the vertical material flow was still strenuous and hook defect probably remained if unreasonable welding parameters with excessive heat input were adopted (Figure 9(c)).

By contrast, the vertical material flow was minimised and the hook defect was eliminated by using the zero-length pin and concave shoulder tool with low heat input conditions (Figure 9(d)). The optimising principle is that the stir pin in the concave shoulder could concentrate plastic material to the weld centre and weaken the material flow around the shoulder periphery during welding. Thus, the effective bonding region around the weld centre was broadened to increase the EBW and the hook defect in the weld periphery was hard to develop.
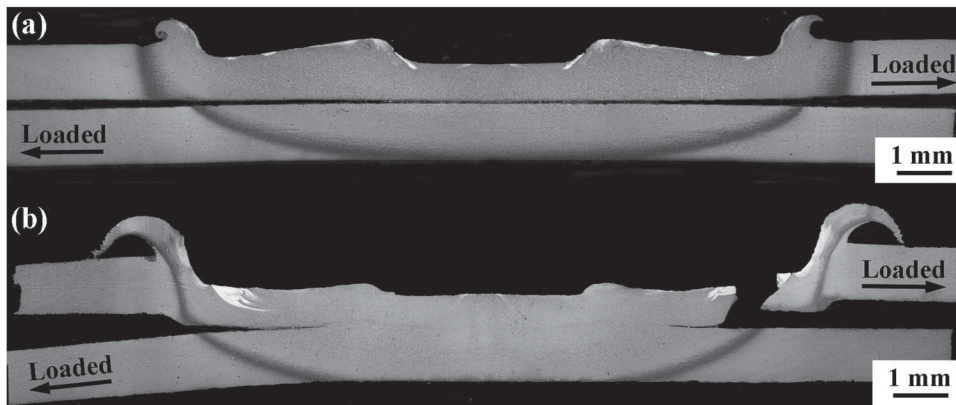
Figure 8. Fractured samples of typical FSSW joints: (a) 600-A, (b) 600-W.
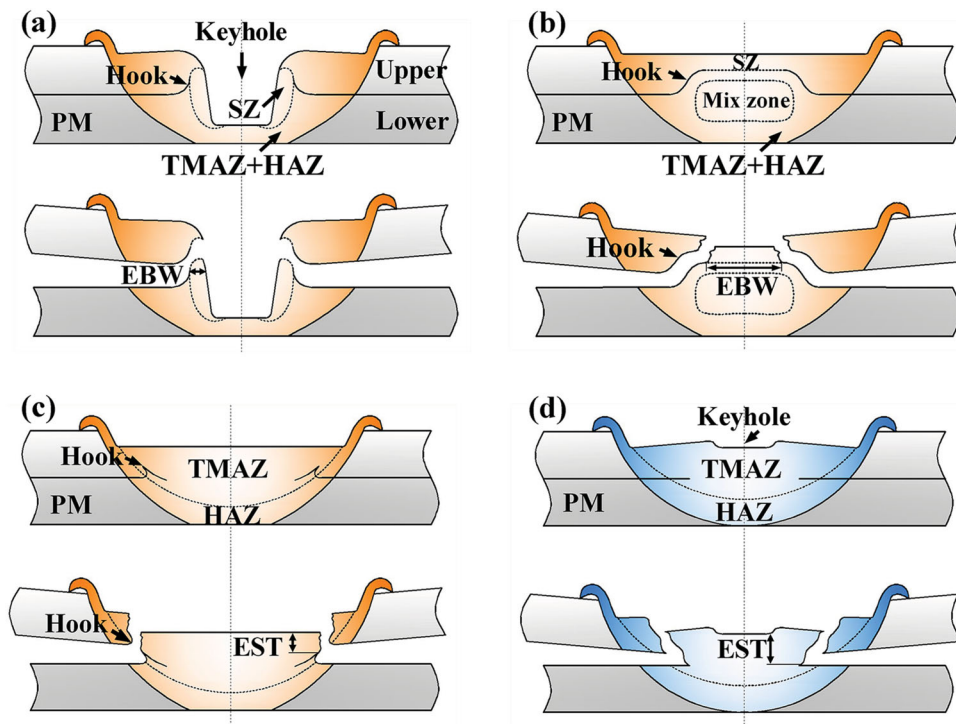
Figure 9. Cross sections and corresponding failure modes of typical FSSW joints with different stir tools: (a) conventional tool with stir pin (SZ means stir zone) [19], (b) re-filling tool [21], (c) pinless tool with high heat input parameters [38], (d) zero-length pin-concave shoulder tool under low heat input conditions.

If the weak bonding was successfully avoided and adequate joining of the interface was achieved (like the 400-W and 600-W joints), the failure would occur at the loaded sheet where endured the maximum thickness reduction or in the HAZ. However, FSSW joints were seldom failed in the HAZ because the joint weakening induced by thickness reduction was more serious than that induced by the HAZ softening. Thus, the EST which reflected the thickness reduction was considered. For pinless FSSW joints, larger EST value could be obtained in our present work (Figure 9(d)), which resulted in relatively higher joint strength than that in high heat input FSSW (Figure 9(c)). Similar relationship could be verified by the superior strength of the 600-W joint compared to that of the 400-W joint.

In addition, the strength variation for the air-cooled and water-cooled joints under the same welding parameter should be clarified (Figure 7(b)). For one thing, the faster cooling rate facilitated the grain refinement and the formation of untempered martensite, which improved the shear strength of TMAZ for water-cooled joints. Wahid et al. [39] summarised that the cooling rate of water-cooled FSW could be enhanced because of the higher thermal capacity and thermal conductivity of water (0.6084 W $(m^{-1} K^{-1})$ at 27°C) than that of the air (0.0260 W $(m^{-1} K^{-1})$ at 27°C). In the work of FSSWed TRIP steel, Mostafapour et al. [40] verified that finer martensite could form in water-cooled joint comparing in-air joint, which was attributed to the lower peak temperature and higher cooling rate by using water cooling.

For another thing, the stir tool was heated to a very high temperature and softened under welding heat effect during the air cooling process. With increasing

the shoulder plunge depth to the preset value, the plastic deformation of the tool occurred by the unceasing rise of temperature, and limited forging force was applied to the sheets. In comparison, the softening and deformation of the stir tool could be availably restrained during water cooling. The larger forging force could be applied to the sheets by the harder tool and sufficient interfacial deformation and metallurgical bonding were confirmed. Thus, more obvious oxide films were found in air-cooled joints due to weak/missing metallurgical bonding (see Figures 3 and 8), and this is another reason why the strength of the air-cooled joint was lower than of the water-cooled joint.

Conclusions

DP1180 steel sheets were joined by the FSSW technique with a specially designed tool with the rotation speeds of 400 and 600 rev min^{-1} under air cooling and water cooling, respectively. The microstructure and mechanical properties of the joints were investigated in detail. The main conclusions are summarised as follows:

(1) No hook defect and obvious keyhole were formed in spot joints by using a concave shoulder tool with zero-length pin. Better joint forming and appearance were obtained under water cooling condition.
(2) Three regions of TMAZ, HAZ and PM were observed in all joints. The HAZ could be particularly partitioned into three sub-zones including the FG-HAZ, IC-HAZ and SC-HAZ. Full martensite was generated in both the TMAZ and FG-HAZ with different grain sizes. DP structures of ferrite and martensite were found in the IC-HAZ and SC-HAZ which underwent temperatures of $A_{c1}-A_{c3}$ and below A_{c1}, during welding, respectively.
(3) The mechanical properties of water-cooled joints were significantly improved, and the maximum lap shear strength was up to 17.9 kN. The ameliorated softening of the HAZ was attributed to the effective control of martensite tempering. Pullout failure samples with higher bonding strength were produced for water-cooled joints while interfacial failure was found in air-cooled joints.

Disclosure statement

No potential conflict of interest was reported by the authors.

Funding

References

[1] Schmitt JH, Iung T. New developments of advanced high-strength steels for automotive applications. C R Phys. 2018;19:641–656.

[2] Pouranvari M, Marashi SPH. Critical review of automotive steels spot welding: process, structure and properties. Sci Technol Weld Join. 2013;18:361–403.

[3] Chabok A, van der Aa E, De Hosson JTM, et al. Mechanical behavior and failure mechanism of resistance spot welded DP1000 dual phase steel. Mater Des. 2017;124:171–182.

[4] Gao S, Li Y, Yang L, et al. Microstructure and mechanical properties of laser-welded dissimilar DP780 and DP980 high-strength steel joints. Mater Sci Eng A. 2018;720:117–129.

[5] Ahiale GK, Oh YJ. Microstructure and fatigue performance of butt-welded joints in advanced high-strength steels. Mater Sci Eng A. 2014;597:342–348.

[6] Lee JH, Park SH, Kwon HS, et al. Laser, tungsten inert gas, and metal active gas welding of DP780 steel: comparison of hardness, tensile properties and fatigue resistance. Mater Des. 2014;64:559–565.

[7] Wang JF, Yang LJ, Sun MS, et al. A study of the softening mechanisms of laser-welded DP1000 steel butt joints. Mater Des. 2016;97:118–125.

[8] Matsushita M, Kitani Y, Ikeda R, et al. Development of friction stir welding of high strength steel sheet. Sci Technol Weld Join. 2011;16:181–187.

[9] Mishra RS, Ma ZY. Friction stir welding and processing. Mater Sci Eng R. 2005;50:1–78.

[10] Saunders N, Miles M, Hartman T, et al. Joint strength in high speed friction stir spot welded DP 980 steel. Int J Precis Eng Manuf. 2014;15:841–848.

[11] Xue P, Xiao BL, Zhang Q, et al. Achieving friction stir welded pure copper joints with nearly equal strength to the parent metal via additional rapid cooling. Scr Mater. 2011;64:1051–1054.

[12] Wang BB, Chen FF, Liu F, et al. Enhanced mechanical properties of friction stir welded 5083Al-H19 joints with additional water cooling. J Mater Sci Technol. 2017;33:1009–1014.

[13] Zeng XH, Xue P, Wang D, et al. Realising equal strength welding to parent metal in precipitation-hardened Al-Mg-Si alloy via low heat input friction stir welding. Sci Technol Weld Join. 2018;23:478–486.

[14] Wang BB, Xue P, Xiao BL, et al. Achieving equal fatigue strength to base material in a friction stir welded 5083-H19 aluminium alloy joint. Sci Technol Weld Join. 2019: 1–8. DOI:10.1080/13621718.2019.1630571.

[15] Wu LH, Hu XB, Zhang XX, et al. Fabrication of high-quality Ti joint with ultrafine grains using submerged friction stirring technology and its microstructural evolution mechanism. Acta Mater. 2019;166:371–385.

[16] Zhang H, Wang D, Xue P, et al. Achieving ultra-high strength friction stir welded joints of high nitrogen stainless steel by forced water cooling. J Mater Sci Technol. 2018;34:2183–2188.

[17] Yin YH, Ikuta A, North TH. Microstructural features and mechanical properties of AM60 and AZ31 friction stir spot welds. Mater Des. 2010;31:4764–4776.

[18] Badarinarayan H, Shi Y, Li X, et al. Effect of tool geometry on hook formation and static strength of friction stir spot welded aluminum 5754-O sheets. Int J Mach Tools Manuf. 2009;49:814–823.

[19] Ohashi R, Fujimoto M, Mironov S, et al. Effect of contamination on microstructure in friction stir spot welded DP590 steel. Sci Technol Weld Join. 2009;14:221–227.

[20] Feng ZQ, Santella ML, David SA. Friction stir spot welding of advanced high-strength steels: a feasibility study. Steel. 2005;66:2130–2136.

[21] Uematsu Y, Tokaji K, Tozaki Y, et al. Effect of re-filling probe hole on tensile failure and fatigue behaviour of friction stir spot welded joints in Al–Mg–Si alloy. Int J Fatigue. 2008;30:1956–1966.

[22] Tozaki Y, Uematsu Y, Tokaji K. A newly developed tool without probe for friction stir spot welding and its performance. J Mater Process Technol. 2010;210:844–851.

[23] Miles MP, Ridges CS, Hovanski Y, et al. Impact of tool wear on joint strength in friction stir spot welding of DP 980 steel. Sci Technol Weld Join. 2011;16:642–647.

[24] Rai R, De A, Bhadeshia HKDH, et al. Review: friction stir welding tools. Sci Technol Weld Join. 2013;16:325–342.

[25] Khan MI, Kuntz ML, Su P, et al. Resistance and friction stir spot welding of DP600: a comparative study. Sci Technol Weld Join. 2007;12:175–182.

[26] Sarkar R, Pal TK, Shome M. Microstructures and properties of friction stir spot welded DP590 dual phase steel sheets. Sci Technol Weld Join. 2014;19:436–442.

[27] Ji SD, Li ZW. Reducing the hook defect of friction stir lap welded alloy by slightly penetrating into the lower sheet. J Mater Eng Perform. 2017;26:921–930.

[28] Li ZW, Yue YM, Ji SD, et al. Joint features and mechanical properties of friction stir lap welded alclad 2024 aluminum alloy assisted by external stationary shoulder. Mater Des. 2016;90:238–247.

[29] Wang ZW, Xie GM, Wang D, et al. Microstructural evolution and mechanical behavior of friction-stir-welded DP1180 advanced ultrahigh strength steel. Acta Metall Sin (Engl Lett). 2019: 1–9. DOI:10.1007/s40195-019-00949-5.

[30] Sackl S, Clemens H, Primig S. Investigation of the self tempering effect of martensite by means of atom probe tomography. Prakt Metallogr-Pract Metallogr. 2015;52:374–383.

[31] Zhang C, Cui L, Wang DP, et al. The heterogeneous microstructure of heat affect zone and its effect on creep resistance for friction stir joints on 9Cr-1.5 W heat resistant steel. Scr Mater. 2019;158:6–10.

[32] Santella M, Hovanski Y, Frederick A, et al. Friction stir spot welding of DP780 carbon steel. Sci Technol Weld Join. 2013;15:271–278.

[33] Xie GM, Cui HB, Luo ZA, et al. Effect of rotation rate on microstructure and mechanical properties of friction stir spot welded DP780 steel. J Mater Sci Technol. 2016;32:326–332.

[34] Ohashi R. Henry Granjon prize competition 2010 winner category a: "joining and fabrication technology" study on friction stir spot welding of dual-phase high-strength steel sheets. Weld World. 2011;55:2–11.

[35] Aldanondo E, Taboada A, Arruti E, et al. Friction stir spot welding of DP1200 steel. In: H Fujii, editor. Proceedings of the 1st international joint symposium on joining and welding; Nov 6-8. Osaka: Woodhead Publishing; 2013. p. 179–182.

[36] Zeng XH, Xue P, Wang D, et al. Effect of processing parameters on plastic flow and defect formation in friction-stir-welded aluminum alloy. Metall Mater Trans A. 2018;49A:2673–2683.

[37] Zeng XH, Xue P, Wang D, et al. Material flow and void defect formation in friction stir welding of aluminium alloys. Sci Technol Weld Join. 2018;23:677–686.

[38] Bakavos D, Chen Y, Babout L, et al. Material interactions in a novel pinless tool approach to friction stir spot welding thin aluminum sheet. Metall Mater Trans A. 2011;42A:1266–1282.

[39] Wahid MA, Khan ZA, Siddiquee AN. Review on underwater friction stir welding: a variant of friction stir welding with great potential of improving joint properties. Trans Nonferrous Met Soc China. 2018;28:193–219.

[40] Mostafapour A, Ebrahimpour A, Saeid T. Numerical and experimental study on the effects of welding environment and input heat on properties of FSSWed TRIP steel. Int J Adv Manuf Technol. 2017;90:1131–1143.